Supporting Information for Graphendofullerene: a novel molecular two-dimensional ferromagnet

Diego López-Alcalá[1], Ziqi Hu[2] and José J. Baldoví[1,*]

[1]Instituto de Ciencia Molecular, Universitat de València, 46980 Paterna, Spain.

[2]Key Laboratory of Precision and Intelligent Chemistry, Collaborative Innovation Center of Chemistry for Energy Materials (iChEM), Department of Materials Science and Engineering, University of Science and Technology of China, Hefei 230026, China.

Table of Contents

1) Pristine C_{80} calculations

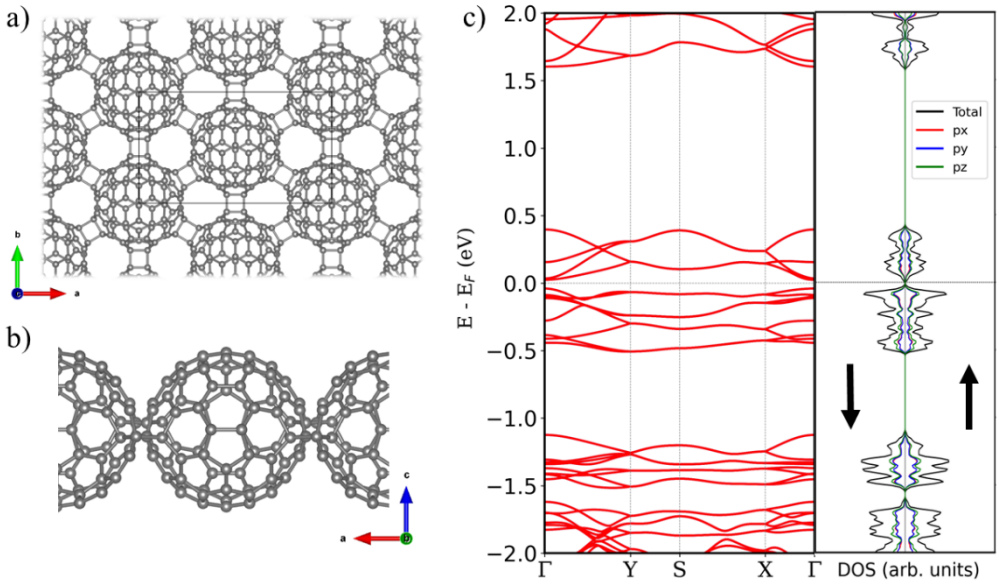

Figure S1: a) Top and **b)** side view of C_{80} graphullerene. **C)** Electronic band structure (left) and projected density of states (PDOS) (right) for C_{80} monolayer. Blue (red) color in a) represents spin up (down) electrons.

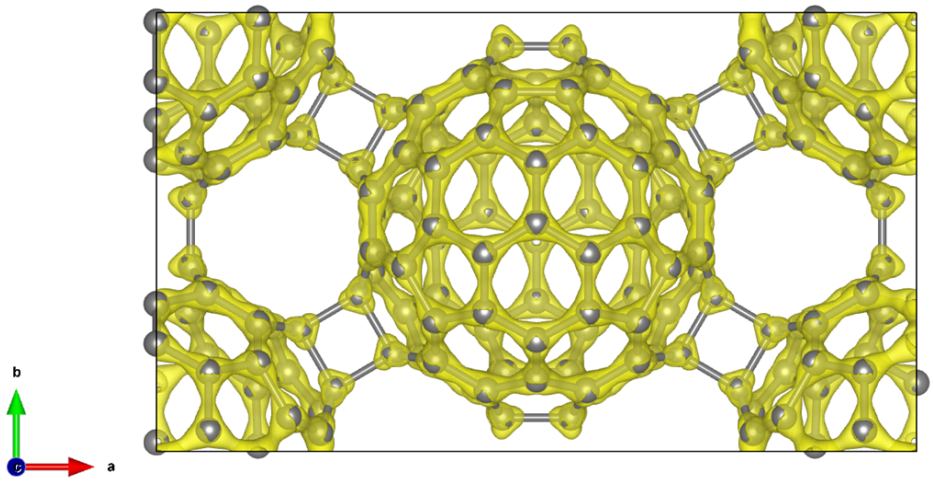

Figure S2: Electronic density of pristine C_{80} monolayer.

2) Additional $V_3N@C_{80}$ calculations

2.1) *Ab-initio* molecular dynamics (AIMD)

We performed AIMD simulations on the fully optimized $V_3N@C_{80}$ structure during 9 ps using a time step of 1 fs at different temperatures (5, 300 and 600 K). We monitored the

evolution of energy and the structure of the system during the simulations, where we found that the morphology of the network remains stable during the simulations, revealing robust mechanical and dynamical stability.

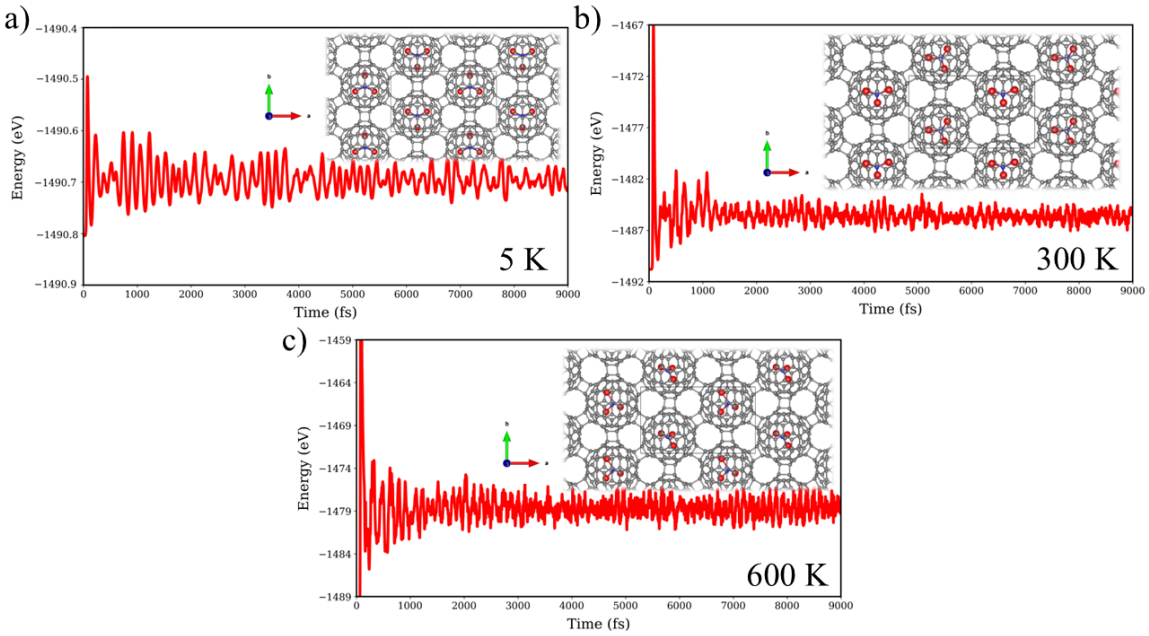

Figure S3: Energy evolution during AIMD at **a)** 5 K, **b)** 300 K and **c)** 600 K. Inset: structure snapshot during AIMD simulations.

2.2) Phonon calculations

We simulated the phonon dispersion of $V_3N@C_{80}$ (Figure S4). The phonon band structure exhibits some imaginary frequencies with slight negative frequency values around the Γ point due to numerical error. This is a well-known issue when dealing with phonon calculations in 2D materials and usually attributed to numerical inaccuracies during the simulations, small residual stress in the system and the size of the supercell,[1,2] so this cannot be considered as a sign of kinetic instability. Indeed, we performed phonon calculations in the $ScV_2N@C_{80}$ relaxed structures (Figures S12), in which the endohedral fullerene building blocks have been experimentally synthesized,[3] to compare the results with the ones founded in the proposed $V_3N@C_{80}$. There, one can see that the same behavior around Γ point is present on the $ScV_2N@C_{80}$ monolayers, confirming the

inability of this state-of-the-art methodology to describe the surrounding of Γ point properly. This can also be observed in the reported phonon band structure of the related material $Sc_3N@C_{80}$ (see Figure 1c-d of Zhao *et al.* [4]).

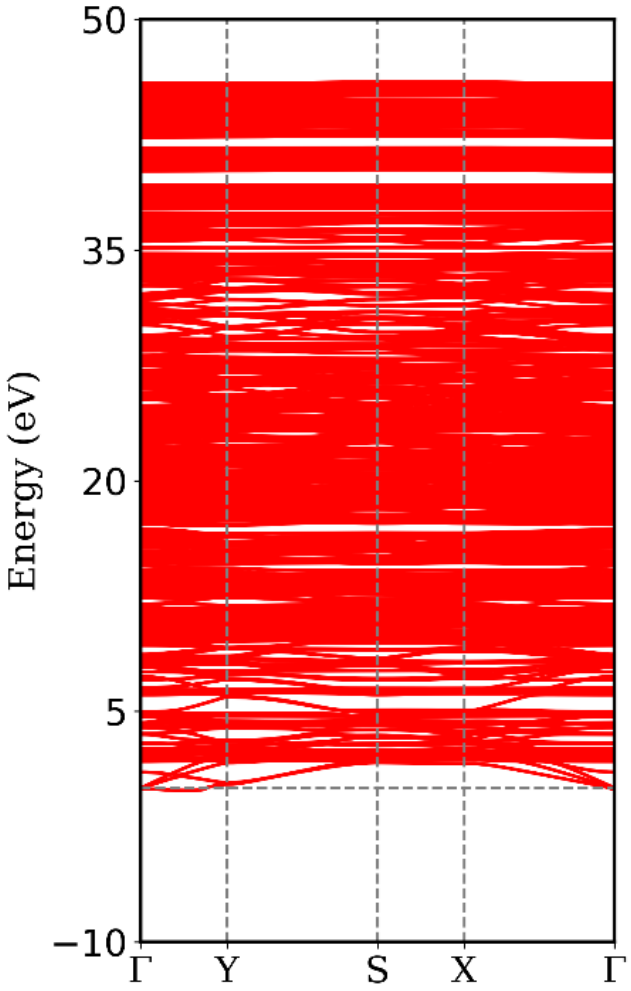

Figure S4: Phonon dispersion of $V_3N@C_{80}$.

2.3) Magnetic exchange interactions

Table S1: Relative energy of the different magnetic configurations of $V_3N@C_{80}$ in meV reported in Figure 2, with respect to the most stable one (E_{FM}).

E_{FM}	$E_{AFM\ single\text{-}stripe}$	$E_{AFM\ double\text{-}stripe}$	$E_{AFM\ zig\text{-}zag}$
0	23	15	27

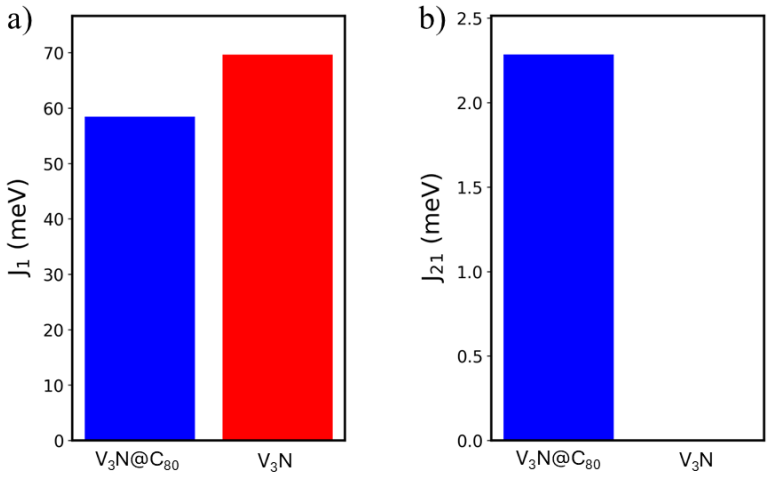

Figure S5: Values of **a)** J_1 and **b)** J_{21} for V_3N inside of C_{80} (blue) and as free-standing molecular arrangement (red) in meV.

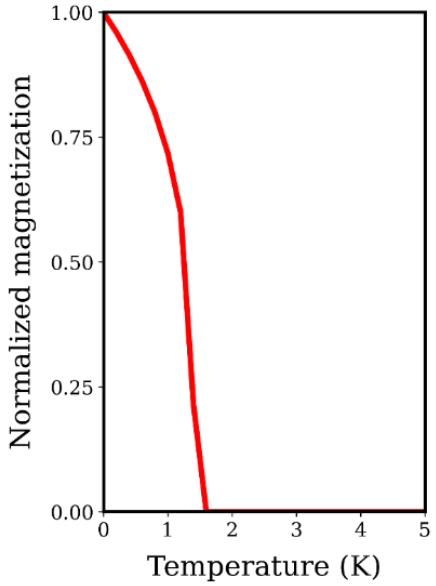

Figure S6: Simulated Curie temperature for $V_3N@C_{80}$ monolayer just taking into account the intramolecular magnetic interactions (J_1) in spin Hamiltonian.

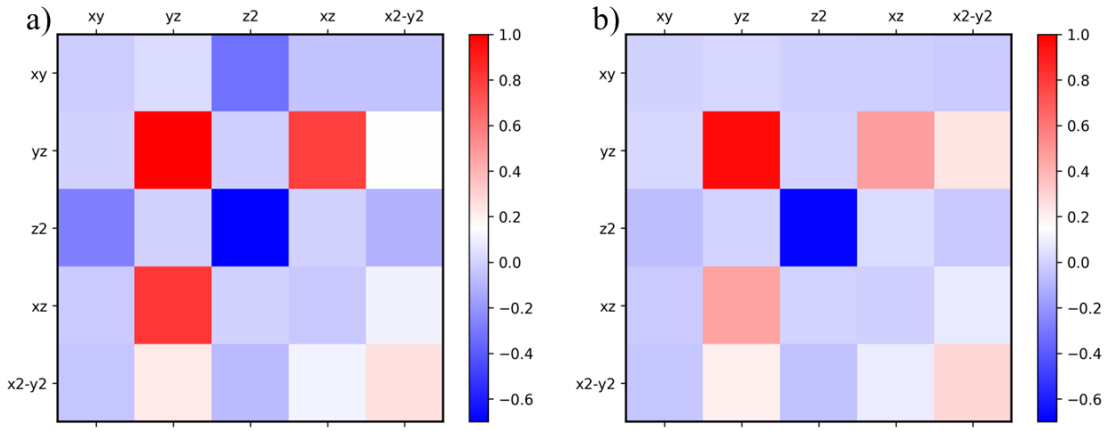

Figure S7: Orbital contribution to J_{21} from first neighbor V atoms at **a)** -4% and **b)** 4% strain.

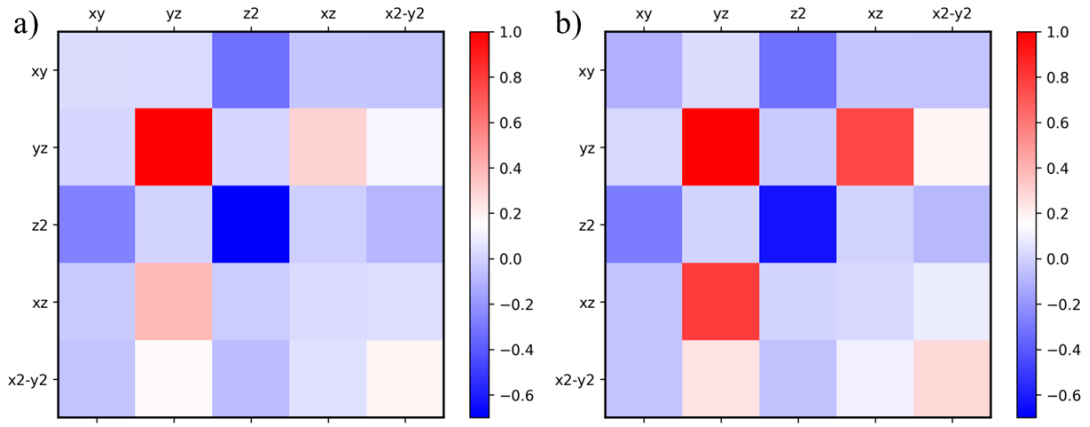

Figure S8: Orbital contribution to J_{21} from first neighbor V atoms at **a)** -3.24x10^{13} cm^{-2} and **b)** 3.24x10^{13} cm^{-2} carrier density. A positive (negative) sign of the carrier density is equivalent to an excess of holes (electrons).

2.4) K-points mesh convergence

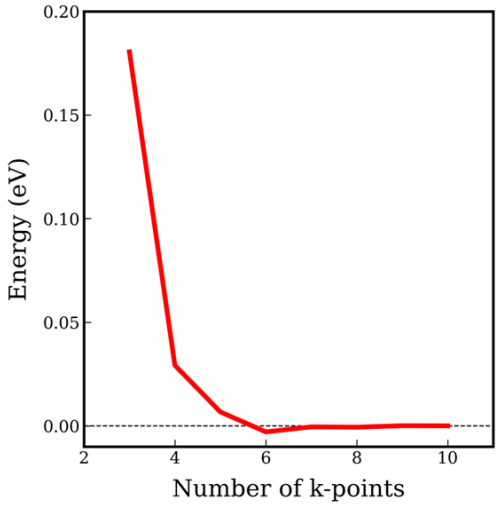

Figure S9: K-point mesh energy convergence for $V_3N@C_{80}$.

3) $ScV_2N@C_{80}$ calculations

We also test the influence on the magnetic properties of substituting V by Sc atoms in the trimetallic nitride molecules, as endohedral metallofullerenes based on Sc_3N, VSc_2N and V_2ScN have already been synthesized.[3] In particular, we determine the magnetic exchange interactions using two structural models (Figure S10a and S11a) based on $V_2ScN@C_{80}$ graphendofullerene, as the introduction of the Sc atoms induces structural anisotropy in the network depending on molecular orientations. Our simulations reveal that, contrary to V_3N, antiferromagnetic coupling between adjacent molecules is favored, and a decrease of the absolute strength of both intra- and intermolecular magnetic coupling takes place (Figures S10(b-d) and S11(b-d)). However, the introduction of Sc atoms does not quench long-range magnetism in the system, which may encourage the experimental preparation of magnetic $V_2ScN@C_{80}$ graphendofullerene.

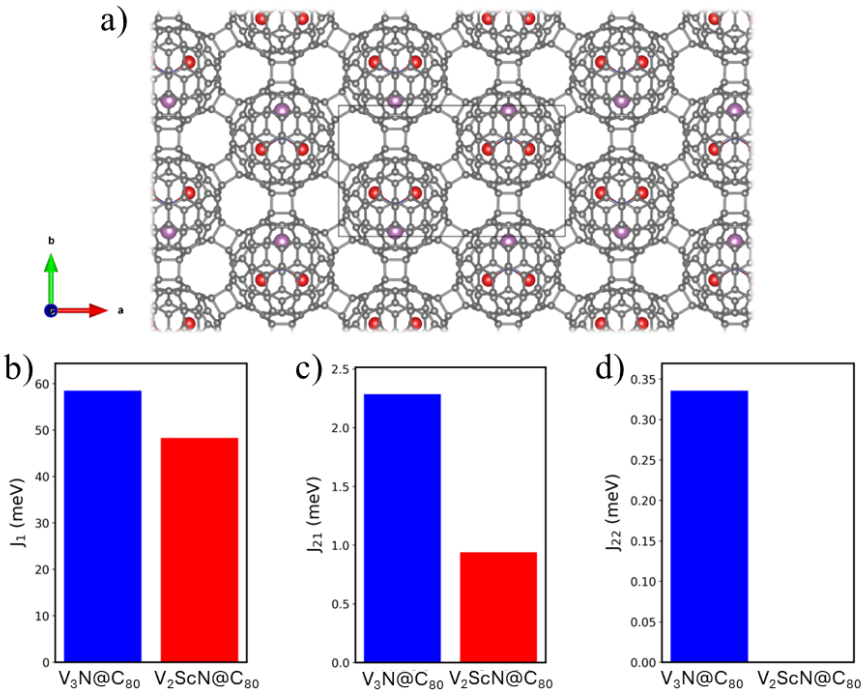

Figure S10: a) Structure of model 1 of $V_2ScN@C_{80}$ graphendofullerene. Color code: carbon (grey), blue (nitrogen), red (vanadium) and purple (scandium). Calculated **b)** J_1, **c)** J_{21} and **d)** J_{22} in meV and comparation with $V_3N@C_{80}$.

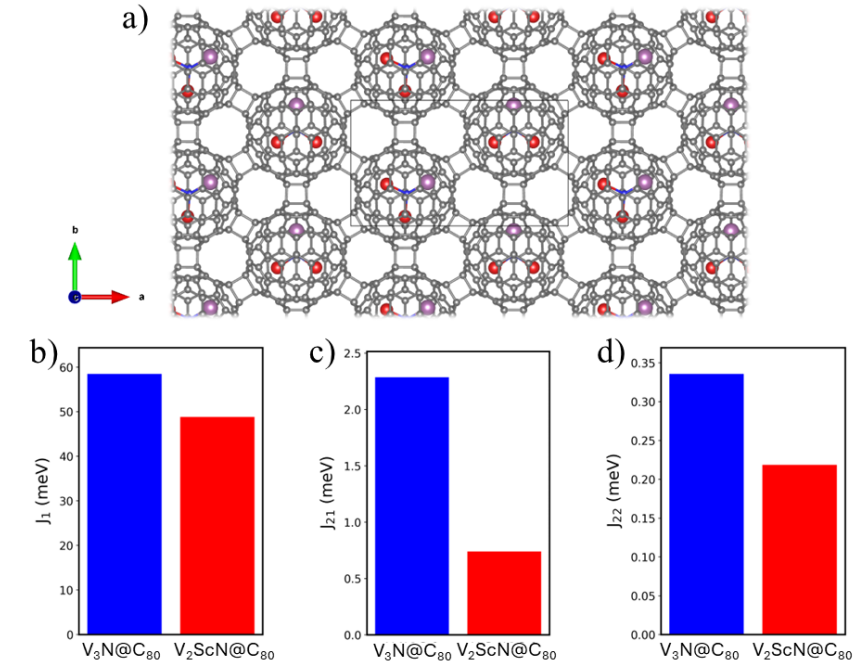

Figure S11: a) Structure of model 2 of $V_2ScN@C_{80}$ graphendofullerene. Color code: carbon (grey), blue (nitrogen), red (vanadium) and purple (scandium). Calculated **b)** J_1, **c)** J_{21} and **d)** J_{22} in meV and comparation with $V_3N@C_{80}$.

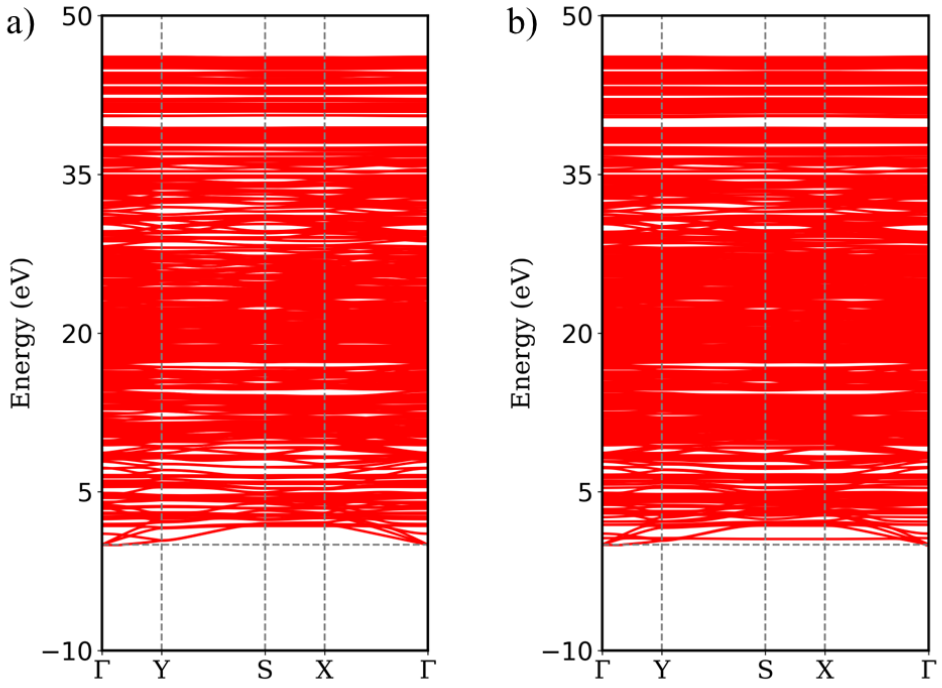

Figure S12: Phonon dispersion of **Sc**V_2N@C_{80} model a) 1 and b) 2.

4) DFT+U

We did not consider Hubbard U corrections in our calculations since the d orbitals of V were delocalized at the Fermi level (Figure S14), so penalties on the occupations of these orbitals are meaningless.[5] We checked the influence of this parameter to corroborate this, where we observe that the pathway that mediates intermolecular interactions is not changed after the introduction of DFT+U corrections (Figure S13). Table S2 shows the magnetic properties of V_3N@C_{80} using different U values, where one can see that this parameter does not affect critically intermolecular interactions, whereas in J_1 the changes are larger since the intramolecular nature of the exchange. Hubbard U corrections decrease the magnetic response of the system as expected since via the inclusion of Coulomb repulsions on d orbitals quenches the hopping between magnetic atoms. We recomputed the Curie temperature and hysteresis loop of V_3N@C_{80} with U = 1, 2 and 3 eV (Figures S15 and S16). Here one can see that the influence of Hubbard U corrections decreases the magnetic response of the material, but the robust ferromagnetism remains present in the network.

Table S2: Magnetic exchange couplings (J), magnetic moments of V atoms and J/μ_B ratios for $V_3N@C_{80}$ monolayer for different Hubbard U values.

	U (eV)			
	0	**1**	**2**	**3**
J_1 (meV)	58.53	44.43	34.87	30.86
J_{21} (meV)	2.28	1.68	1.24	0.46
Magnetic moment (μ_B)	2.68	2.62	2.56	2.50
J_1/μ_B	21.83	16.99	13.62	12.35
J_{21}/μ_B	0.32	0.25	0.19	0.07

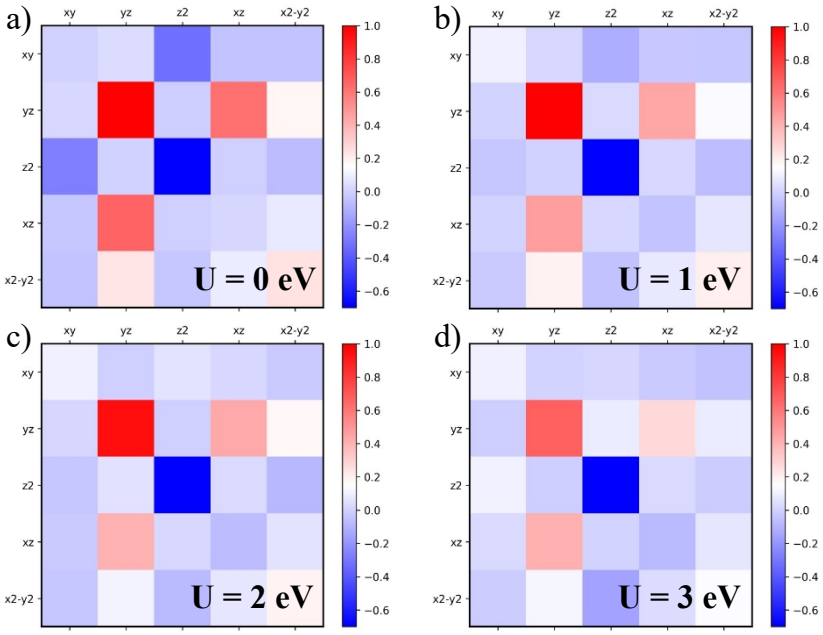

Figure S13: Orbital contribution to J_{21} for Hubbard U values of **a)** 0 **b)** 1 **c)** 2 and **d)** 3 eV in $V_3N@C_{80}$ monolayer.

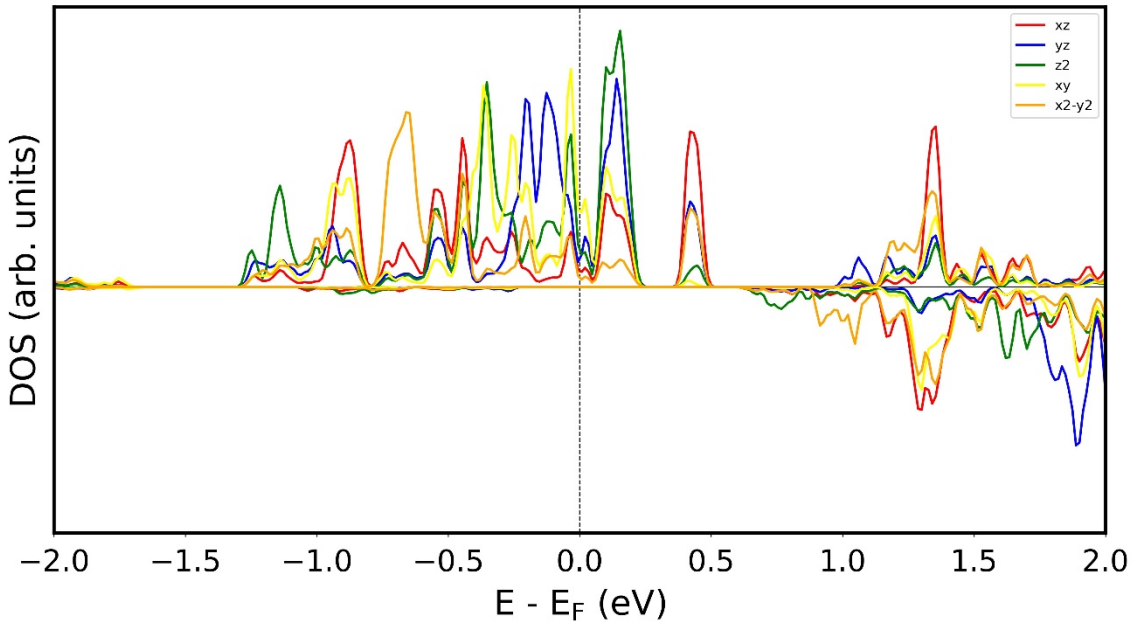

Figure S14: PDOS of d orbitals of V atoms in $V_3N@C_{80}$.

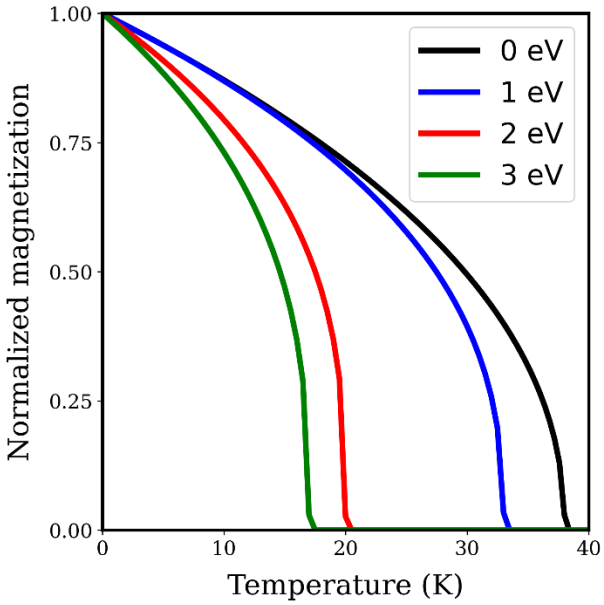

Figure S15: Calculated Curie temperature for $V_3N@C_{80}$ with different Hubbard U values.

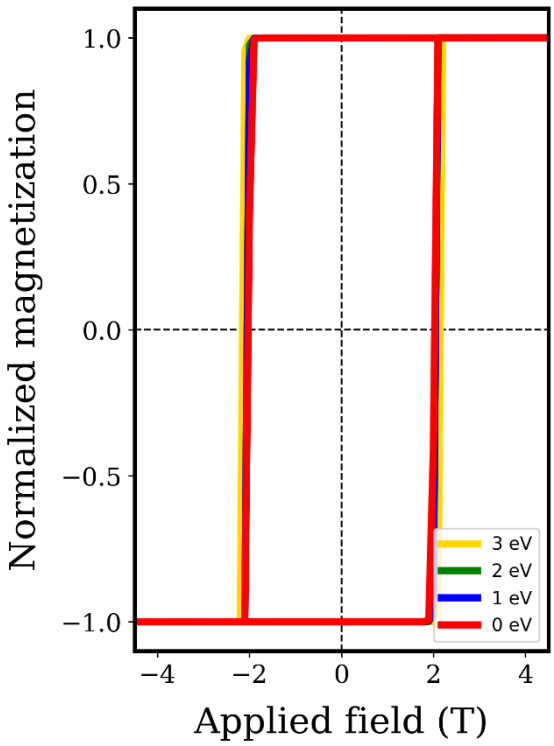

Figure S16: Calculated hysteresis loop for $V_3N@C_{80}$ with different Hubbard U values.

5) Optimized structure and lattice parameters of $V_3N@C_{80}$

a = 17.92321 Å, b = 10.334916 Å, c = 36.0 Å, α = 90º, β = 90º and γ = 90º.

C	0.27078386	4.05797376	17.8755174
C	8.36322071	3.50241002	16.4883244
C	1.39758022	4.45256086	15.7710707
C	7.86445362	5.46484521	17.9346965
C	2.10567248	5.60852121	19.0592078
C	6.81564114	4.08973296	14.6172403
C	2.09283946	4.65541459	20.1269201
C	6.86243865	2.72459391	14.2252373
C	3.32083027	4.84171178	14.3497262
C	5.66034687	6.31263904	18.8381787
C	3.75328148	5.88835973	15.2339869
C	5.28268692	6.94480518	17.523472
C	3.2599272	4.43528088	20.9495855
C	5.70502944	2.08905858	13.6644963
C	0.61611034	3.00905213	18.9017214
C	1.36768431	3.39745895	20.0553354
C	1.8186502	5.52839461	16.6106495
C	3.01083043	6.22793407	16.3811457
C	17.6377291	9.23575634	17.1628797
C	9.5759051	8.68661058	18.5447354
C	16.523479	9.63102554	19.2728079

C	10.0589356	0.28890224	17.1097592
C	15.8292772	0.42986016	15.9823628
C	11.1093253	9.26866272	20.4307495
C	15.8456232	9.83812692	14.9138571
C	11.0646965	7.90482586	20.8319485
C	14.6013581	10.0205279	20.7087939
C	12.2547439	1.14077836	16.214896
C	14.1672221	0.73340698	19.8248939
C	12.6282636	1.80170658	17.5230392
C	14.6710794	9.61418996	14.1021909
C	12.2196323	7.26530126	21.3951418
C	17.3084977	8.193046	16.1310138
C	16.5644873	8.57588229	14.9900579
C	16.1067106	0.37024837	18.4341667
C	14.9258041	1.07589576	18.6703062
C	17.652462	6.27684922	17.8755174
C	9.56000721	6.83241297	16.4882162
C	16.5257015	5.88235514	15.7710707
C	10.0587922	4.87011213	17.9345522
C	15.8174838	4.72644646	19.0591717
C	11.1074972	6.24506936	14.6170961
C	15.8303705	5.67955309	20.126848
C	11.0607714	7.61022908	14.2249849
C	14.6024335	5.49325589	14.3497623
C	12.2629707	4.02225629	18.8382508
C	14.1699285	4.44663895	15.2339869
C	12.6405948	3.39023484	17.5234359
C	14.6633903	5.89963512	20.9496215
C	12.2182702	8.24590909	13.6643521
C	17.30701	7.32592588	18.9017214
C	16.5555257	6.93750873	20.0553354
C	16.1046136	4.80641804	16.6106135
C	14.9123975	4.10703361	16.3811457
C	0.28557051	1.09910798	17.1629879
C	8.3473049	1.64825374	18.5447714
C	1.39976686	0.70386979	19.272844
C	7.86425647	10.0460344	17.1097231
C	2.09400447	9.90512818	15.9823989
C	6.81386675	1.06625328	20.4307855
C	2.07776604	0.49689243	14.9138932
C	6.85854931	2.43005913	20.8319846
C	3.3217802	0.31449149	20.7087579
C	5.66851986	9.19418931	16.214896
C	3.75593412	9.60147802	19.824966
C	5.29498224	8.5332921	17.5230753
C	3.2522023	0.72056068	14.1022991
C	5.7036135	3.06964575	21.3951418
C	0.61473026	2.14179766	16.1309417

C	1.35875855	1.75898203	14.9900218
C	1.81632018	9.96478132	18.4342028
C	2.99747764	9.25899957	18.6703062
C	9.23238886	6.27689056	17.8755534
C	17.3248257	6.83246464	16.4881801
C	10.3591494	5.88229314	15.7710346
C	16.8260407	4.87009146	17.9345883
C	11.0673492	4.72636379	19.0591717
C	15.7772282	6.24509003	14.6170961
C	11.0545878	5.67955309	20.1269201
C	15.8239182	7.61023942	14.225057
C	12.2823636	5.49318355	14.3497262
C	14.6220056	4.02236998	18.8381787
C	12.7149582	4.44668029	15.2339508
C	14.244274	3.39020384	17.5234359
C	12.2216577	5.89962479	20.9496576
C	14.6665448	8.24589876	13.664316
C	9.57775119	7.32593621	18.9017574
C	10.3294327	6.9375294	20.0553354
C	10.7802731	4.80642838	16.6106495
C	11.972525	4.10699227	16.3811817
C	8.67621373	1.09907698	17.1629879
C	0.61431802	1.64824341	18.5446272
C	7.56196361	0.70381812	19.2729161
C	1.09738438	10.0460138	17.1096149
C	6.86770807	9.90505584	15.982471
C	2.14768449	1.06619127	20.4307495
C	6.88401819	0.49679941	14.9139293
C	2.10293023	2.42999713	20.8319846
C	5.63973518	0.31454317	20.7087939
C	3.29313891	9.1941273	16.2148599
C	5.20561711	9.6015917	19.824966
C	3.66658692	8.53327143	17.5230392
C	5.7096357	0.72057101	14.1022991
C	3.25788396	3.06964575	21.3951418
C	8.34696436	2.14177699	16.1310499
C	7.60297191	1.7589717	14.9902382
C	7.14515936	9.96475031	18.434311
C	5.96416321	9.25907191	18.6703062
C	8.69087491	4.0580151	17.8755534
C	0.59849183	3.50235834	16.4882883
C	7.56407855	4.45255052	15.7711789
C	1.09709761	5.46480387	17.9345522
C	6.85589667	5.60853155	19.0592078
C	2.14601763	4.08978463	14.6171321
C	6.86871177	4.65542492	20.126848
C	2.09936351	2.72458357	14.2250931
C	5.64077473	4.84163944	14.3497983

C	3.3013119	6.31263904	18.8381787
C	5.20839521	5.88827705	15.234023
C	3.67895393	6.94473284	17.5234359
C	5.70162403	4.43534289	20.9495855
C	3.25682649	2.08902758	13.6644242
C	8.34556635	3.00894878	18.9018296
C	7.59377731	3.39732459	20.0553714
C	7.14299065	5.52840494	16.6107217
C	5.95082834	6.22796507	16.3811817
C	9.2470142	9.23579768	17.1629158
C	17.3088382	8.68666226	18.5445551
C	10.3613719	9.63111856	19.2728079
C	16.8258794	0.28891258	17.1096149
C	11.0555378	0.42988083	15.9823989
C	15.7755076	9.2687454	20.4307495
C	11.0391918	9.83812692	14.9140014
C	15.8203335	7.90493955	20.8318764
C	12.2834927	10.0204245	20.7087579
C	14.6302682	1.14071635	16.214896
C	12.7176108	0.73346899	19.8248939
C	14.2566231	1.80174792	17.5230753
C	12.2136998	9.61417963	14.102263
C	14.6653798	7.26535293	21.3952139
C	9.57624564	8.193046	16.1310499
C	10.3202381	8.57578928	14.9900218
C	10.7780686	0.37021736	18.4341667
C	11.9590468	1.07591643	18.6702701
C	13.4424792	0.89576851	15.4420334
C	13.4424254	9.38047617	21.2721675
C	13.4424254	10.2840992	14.3664233
C	13.442515	7.98702978	21.5704432
C	4.48085627	9.4390028	15.4419973
C	4.48074873	0.95445016	21.2721315
C	4.48092796	0.05076511	14.3663872
C	4.48073081	2.34793789	21.5703711
C	4.4808025	6.05664317	19.6046581
C	4.48083835	4.20169111	13.7930242
C	4.48076665	5.11495663	20.6779241
C	4.48089212	2.8055473	13.4953616
C	13.4424613	4.27828317	19.6046221
C	13.4424075	6.13321456	13.7929882
C	13.442533	5.2199387	20.6780684
C	13.4424075	7.52954439	13.4952534
V	2.88264363	3.4541873	18.0275943
V	15.0406201	6.8807287	18.0272698
V	11.8442486	6.88081138	18.0271255
V	6.07894344	3.45426998	18.0276665
V	13.4425867	9.54918334	17.1764033

V	4.48091004	0.78569132	17.1763311
N	4.48082042	2.66257407	17.3981536
N	13.4424792	7.67216623	17.3972521

References

1. Zólyomi, V., Drummond, N. D. & Fal'ko, V. I. Electrons and phonons in single layers of hexagonal indium chalcogenides from *ab initio* calculations. *Phys Rev B* **89**, 205416 (2014).

2. Şahin, H. *et al.* Monolayer honeycomb structures of group-IV elements and III-V binary compounds: First-principles calculations. *Phys Rev B* **80**, 155453 (2009).

3. Wei, T. *et al.* Entrapping a Group-VB Transition Metal, Vanadium, within an Endohedral Metallofullerene: $V_x Sc_{3-x} N@I_h\text{-}C_{80}$ (x = 1, 2). *J Am Chem Soc* **138**, 207–214 (2016).

4. Zhao, Y. *et al.* Two-dimensional fullerene-based monolayer materials assembled by C_{80} and $Sc_3N@C_{80}$. *Physical Chemistry Chemical Physics* **26**, 10841–10849 (2024).

5. Himmetoglu, B., Floris, A., de Gironcoli, S. & Cococcioni, M. Hubbard-corrected DFT energy functionals: The LDA+U description of correlated systems. *Int J Quantum Chem* **114**, 14–49 (2014).